


Free Energy Calculations on the Two Drug Binding Sites in the M2 Proton Channel

Ruo-Xu Gu,[†] Limin Angela Liu,^{*,#} Dong-Qing Wei,^{*,†} Jian-Guo Du,[‡] Lei Liu,[‡] and Hong Liu[‡]

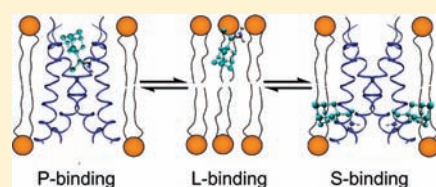
[†]State Key Laboratory of Microbial Metabolism, Luc Montagnier Biomedical Research Institute, and College of Life Sciences and Biotechnology, Shanghai Jiao Tong University, Shanghai Minhang District, China 200240

[#]Fred Hutchinson Cancer Research Center, Seattle WA, 98109, United States

[‡]Institute of Earthquake Science, China Earthquake Administration, Beijing, China 100036

 Supporting Information

ABSTRACT: Two alternative binding sites of adamantane-type drugs in the influenza A M2 channel have been suggested, one with the drug binding inside the channel pore and the other with four drug molecule S-binding to the C-terminal surface of the transmembrane domain. Recent computational and experimental studies have suggested that the pore binding site is more energetically favorable but the external surface binding site may also exist. Nonetheless, which drug binding site leads to channel inhibition *in vivo* and how drug-resistant mutations affect these sites are not completely understood. We applied molecular dynamics simulations and potential of mean force calculations to examine the structures and the free energies associated with these putative drug binding sites in an M2–lipid bilayer system. We found that, at biological pH (~ 7.4), the pore binding site is more thermodynamically favorable than the surface binding site by ~ 7 kcal/mol and, hence, would lead to more stable drug binding and channel inhibition. This result is in excellent agreement with several recent studies. More importantly, a novel finding of ours is that binding to the channel pore requires overcoming a much higher energy barrier of ~ 10 kcal/mol than binding to the C-terminal channel surface, indicating that the latter site is more kinetically favorable. Our study is the first computational work that provides both kinetic and thermodynamic energy information on these drug binding sites. Our results provide a theoretical framework to interpret and reconcile existing and often conflicting results regarding these two binding sites, thus helping to expand our understanding of M2–drug binding, and may help guide the design and screening of novel drugs to combat the virus.



1. INTRODUCTION

Extensive experimental and computational studies have been carried out to elucidate the structure and function of the influenza A M2 proton channel^{1–23} (briefly reviewed in the Supporting Information and summarized in Table 1) that is critical for the viral life cycle. Two adamantane-based antiviral drugs, amantadine and rimantadine (Figure S1C, Supporting Information), which inhibit the M2 channel, have been approved for treating influenza A viral infections.^{1,2,24} However, the virus has quickly obtained drug resistance^{8,9,25} in a number of naturally occurring M2 mutant strains due to the fast mutation rate of the M2 protein. Therefore, it is essential to understand how these drugs bind to the M2 channel and inhibit its proton conduction as well as how mutations affect drug binding so that better drugs may be found or designed.

Two alternative binding sites of amantadine and rimantadine in the M2 channel have been reported recently, with one amantadine molecule bound in the channel pore (pore binding or P-binding) of a G34A M2 mutant at an environmental pH of 5.3 by crystallography²⁶ (PDB ID 3C9J) and with four molecules of rimantadine bound at the C-terminal surface of the transmembrane domain of the M2 channel (surface binding or S-binding) at pH 7.5 by solution NMR (sNMR)²⁷ (PDB ID 2RLF). Both models have received support from experimental

and computational studies (reviewed in the Supporting Information), with the P-binding site being more widely accepted in the literature.

These two 3D structures demonstrated two different drug binding conformations, suggested two possible inhibition mechanisms, and provided two alternative rationales for drug resistance in the S31N mutant.²⁸ In the former pore binding model, the drug molecule occludes the pore and prevents protons from conducting, thus inhibiting normal channel function.²⁶ Mutation S31N was believed to cause the pore size to decrease so that the drug molecule no longer binds in the pore.¹³ In the latter surface binding model, the drug molecules stabilize the closed conformation of the channel and may inhibit proton transfer by an allosteric mechanism proposed by Schnell and Chou.²⁷ In the S31N mutant, the S-binding sites are allosterically perturbed so that drug molecules no longer bind effectively, thus leading to drug resistance.²⁷

Since the discovery of these two alternative drug binding sites, a series of experimental and computational studies have been carried out to investigate and compare these sites.^{13,16–23,29–33}

Received: December 19, 2010

Published: June 28, 2011

Table 1. Summary of the Experimentally Solved Structures of the M2 Channel in the Protein Data Bank^a

PDB ID	environment	pH	X-ray or NMR	form	drug concn	M2 protein length	mutation	pore-facing residues	helix tilt angle (deg)	ref
1NYJ	DMPC bilayer	7.0	ssNMR	apo form		Ser22–Leu46		Val27, Ser31, Gly34, His37, Trp41	~38	67
2H9S	DMPC bilayer	8.8	ssNMR	apo form		Ser22–Leu46		Val27, Ala30, Gly34, His37, Trp41	~28 (N), ~19 (C) ^b	57
2KAD	DLPC bilayer	7.5	ssNMR	amantadine	M2:DLPC:amantadine = 1:1.5:8 (M)	Ser22–Leu46		Val27, Ser31, Gly34, His37, Trp41	~38	17
2KQT	DMPC bilayer	7.5	ssNMR	amantadine	same as that for 2KAD	Ser22–Leu46		Val27, Gly34, His37, Trp41, Ser31 ^c , Ala30 ^c	~30 (N), ~19 (C) ^b	33
3C9J	PEG/OG bilayer-like	5.3	X-ray (3.5 Å)	amantadine	M2:amantadine = 4:3 (M)	Ser22–Leu46	G34A	Val27, Ser31, Ala34, His37, Trp41	~35	26
3BKD	PEG/OG bilayer-like	7.3	X-ray (2.0 Å)	apo form		Ser22–Leu46	I33-SeaMet	Val27, Ser31, Gly34, His37, Trp41	~35	26
2RLF	DHPC micelles	7.5	solution NMR	rimantadine	M2:DHPC:rimantadine = 0.75:300:40 (M)	Ser23–Lys60	CS0S	Val27, Ala30, Gly34, His37, Trp41	~23	27
2KIH	DHPC micelles	7.5	solution NMR	apo form		Ser23–Lys60	S31N, C50S	Val27, Ala30, Gly34, His37, Trp41	~23	28
2KWY	DHPC micelles	7.5	solution NMR	apo form		Ser23–Lys60	V27A, C50S	Ala27, Ala30, Gly34, His37, Trp41	~23	51
2L0J	DOPC/DOPE bilayer	7.5	ssNMR	apo form	M2:DOPC/DOPE = 1:14 (mass)	Ser22–Gly62	CS0S	Val27, Gly34, His37, Trp41, Ser31 ^c , Ala30 ^c	~32 (N), ~22 (C) ^b	52

^a Abbreviations: DHPC, 1,2-dihexanoyl-*sn*-glycero-3-phosphatidylcholine; DLPC, 1,2-dilauroyl-*sn*-glycero-3-phosphatidylcholine; DMPC, 1,2-dimyristoyl-*sn*-glycero-3-phosphatidylcholine; DOPC, 1,2-dioleoyl-*sn*-glycero-3-phosphatidylcholine; DOPE, 1,2-dioleoyl-*sn*-glycero-3-phosphatidylethanolamine; M2-TMD, transmembrane part of the M2 protein; OG, octyl β -D-glucopyranoside; PEG, polyethylene glycol; ssNMR, solid-state NMR. ^b N means N-terminal, and C means C-terminal. ^c Partially facing the pore and partially facing the interhelical regions.

Table 2. Starting Structures for the Six Molecular Dynamics Simulations Carried out in This Study for the Wild Type and the S31N Mutant of the M2 channel^a

	apo form	pore binding form	surface binding form
wild type (WT)	PDB structure (ID 2RLF) with rimantadine molecules removed	one rimantadine molecule docked to the channel pore of the WT apo form using AutoDock	PDB structure (ID 2RLF)
S31N mutant	equilibrated WT apo form with Ser31 mutated to Asn	equilibrated WT pore binding form with Ser31 mutated to Asn	equilibrated WT surface binding form with Ser31 mutated to Asn

^aThe three forms of the M2 channel include the apo form, the pore binding form, where one rimantadine molecule is bound in the channel pore, and the surface binding form, where four rimantadine molecules are bound at the C-terminal surface of the channel.

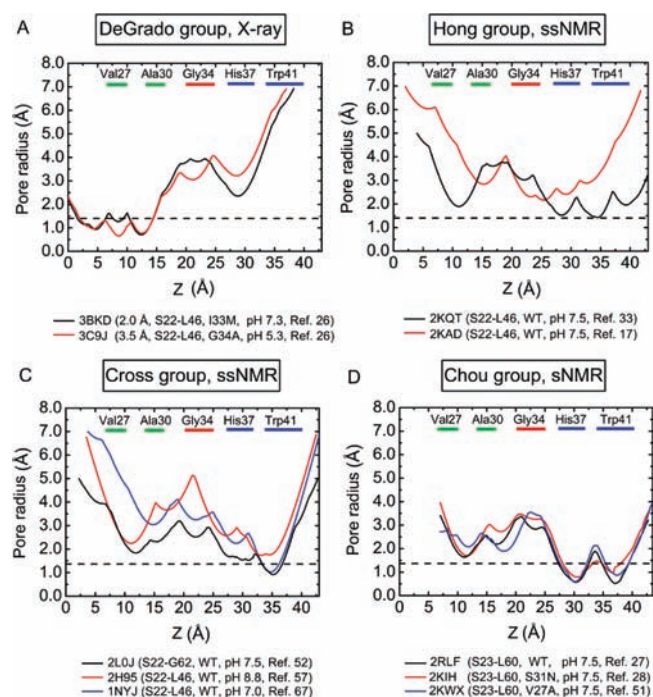


Figure 1. Pore radius profiles of experimentally solved M2 structures in Table 1. Structures solved by four research groups are shown in separate panels. Z represents the channel helix. The approximate positions of five key pore-lining residues are labeled at the top by bars with different colors. Val27 and Ala30, which form the N-terminal hydrophobic gate, are labeled in green, whereas His37 and Trp41, which form the C-terminal gate, are labeled in blue. The position of Gly34 at the pore is labeled in red. The horizontal dashed line at 1.4 Å in all panels represents the radius of a water molecule. The structure resolution (Å; for X-ray), the M2 protein chain length and mutational state, the experimental pH value, and the published reference of each structure are shown beside the PDB entry ID. sNMR and ssNMR refer to solution NMR and solid-state NMR, respectively. WT refers to the wild type. The pore radius profiles were calculated by HOLE2.⁵³

Cady et al.³³ found that both binding sites were possible by solid-state NMR (ssNMR) experiments, with the channel pore the preferable binding site and the C-terminal surface a secondary binding site at high concentrations of amantadine. Chuang et al.²⁹ applied the hot spot screening method by solvent mapping and found that the P-binding site was energetically more favorable and believed to play a dominant role in channel inhibition but the S-binding site was another valid drug binding site that could exist under appropriate conditions. Rosenberg et al.³⁰ demonstrated that both

binding sites may exist and the adamantane drugs have a significantly higher binding affinity for the P-binding site through a series of surface plasmon resonance (SPR) experiments. Kozakov et al.³⁴ argued that both binding sites should be considered to reconcile existing experimental results that often seem contradictory. These recent studies suggest that investigating both binding sites is important to achieve complete understanding of the drug inhibition mechanism of the M2 channel. However, which binding site plays a more important role in vivo remains a controversial subject that calls for more in depth analysis.

In this study, we investigated the structural and energetic factors that affect the two drug binding sites of the M2 channel by a series of molecular dynamics (MD) simulations and potential of mean force (PMF) calculations. From the PMF calculations, both kinetic and thermodynamic energy information about drug–M2 binding can be obtained. On the basis of our structural analysis and PMF results, we found the P-binding site to be the thermodynamically favored site that leads to stable drug binding and channel inhibition, consistent with recent studies.^{29–33} In addition, our study is the first to discover that the S-binding site is the kinetically favored site that leads to fast drug binding. These results provide a theoretical framework to reconcile conflicting experimental results in support of either drug binding model by examining the experimental conditions that favor either thermodynamic or kinetic binding.

2. METHODS

Six M2 structures were simulated, three for the wild type (WT) and three for the S31N mutant, including the apo form M2 channel and the P-binding and S-binding forms of the rimantadine–M2 complex structures, as shown in Table 2. Docking was done using AutoDock 3.0.5³⁵ to create M2–drug complex structures. The wild type starting structures were then inserted into a pre-equilibrated DPPC (dipalmitoylphosphatidylcholine) bilayer with 128 lipids.^{36,37} After removal of 10 lipid molecules from each membrane leaflet to remove bad contacts, the systems were then solvated by SPC (single point charge) water molecules. Chloride ions were added to neutralize the systems. The simulation boxes are about (65 Å × 65 Å × 75 Å) in size with a thickness of about 15 Å for solvent on each side of the lipid bilayer. The final systems contain 152 amino acids, 108 lipid molecules, ~4800 water molecules, and 4–8 chloride ions (Figure S1B, Supporting Information). The Z axis of the simulation box is perpendicular to the bilayer and parallel to the central axis of the helix bundle.

Molecular dynamics simulations^{38–41} were performed for these six structures. Potential of mean force calculations^{42–47} were performed to obtain the energy barriers and the binding free energy changes associated with three rimantadine binding reactions. In the first reaction, a

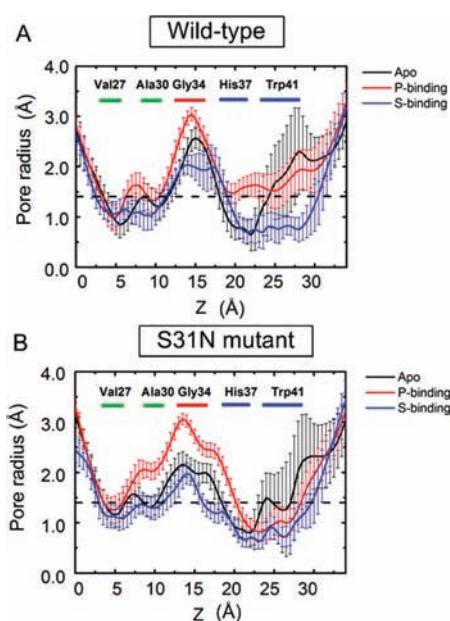


Figure 2. Pore radius profiles of the simulated M2 structures in Table 2. Panel A shows the average pore radii and standard deviations along the pore helix for the three wild type structures, whereas panel B is for the S31N mutant. The apo form (black), the P-binding model (red), and the S-binding model (blue) are shown. Z represents the channel helix. The key pore-lining residues and the radius of a water molecule are shown as in Figure 1. The pore radius profiles were calculated by HOLE2.⁵³

rimantadine molecule enters the channel pore from the N-terminal end of the channel and binds the channel at the P-binding site. In the second reaction, a rimantadine molecule leaves the S-binding site and enters the lipid–water environment. In the third reaction, a solvent-bound rimantadine molecule enters and penetrates the lipid bilayers. The GROMOS united-atom force field³⁸ and Berger’s united-atom force field⁴⁰ were used for describing the protein and the lipids, respectively, in the MD simulations and the PMF calculations. Berger’s united-atom force field was chosen on the basis of its accuracy in describing lipid bilayers. To evaluate the effects of the force field parameters on the accuracy of protein descriptions, we repeated the MD simulations and the PMF calculations using the OPLS all-atom force field for describing the protein and the rimantadine molecules.^{48–50} Detailed simulation protocols and methods for data analysis can be found in the Supporting Information.

3. RESULTS AND DISCUSSION

3.1. Structures of the M2 Channel and the M2–Drug Complexes. To date, 10 structures have been solved for the M2 channel that are summarized in Table 1. The M2 channel has been found to be highly flexible and sensitive to its environment and experimental conditions.^{17,23,45} As a result, it is understandable that the structures in Table 1 varied greatly regarding many properties, such as pore-lining residues, transmembrane helix tilt angle, and pore radius profile (Figure 1). Except for the P-binding amantadine–M2 complex structure (PDB ID 3C9J), all other structures were obtained at neutral pH where the closed-channel conformation of M2 is expected. However, as can be seen from Figure 1, except for the solution NMR structures^{27,28,51} (PDB ID 2RLF for the wild type; PDB ID 2KIH for the S31N mutant, and PDB ID 2KWX for the V27A mutant) and the recent ssNMR structures^{33,52} (PDB IDs 2KQT and 2L0J), which are closed-channel

structures, all other structures appear to be in open-channel conformations whose pore radii⁵³ often exceed the size of amantadine. This may be partly due to the fact that most of these closed-channel structures (PDB IDs 2RLF, 2KIH, 2KWX, and 2L0J) included the C-terminal domain of the channel (Table 1 and Figure S1A, Supporting Information), which was found to be important for the stability of the channel structure.^{46,47} We chose the solution NMR structure²⁷ (PDB ID 2RLF) as the starting structure for molecular modeling. We also note that the pore radius profiles for the transmembrane portion of 2RLF (sNMR) and 2L0J (ssNMR) are highly similar (Figure 1), despite the fact that these two structures were obtained in different environments and the C-terminal helices show different conformations.

3.1.1. Molecular Dynamics Simulation of the Six Model Structures. We carried out molecular dynamics simulations to compare the structural characteristics of the two drug binding models starting from the solution NMR structure (PDB ID 2RLF). Table 2 summarizes the six model structures that we simulated, including the apo form of the M2 channel and the P-binding and S-binding structures of the M2–rimantadine complexes for both the wild type and the S31N mutant. The environmental pH of 7.5 was used for all simulations, as it has been found that the drug molecules bind to the channel more readily when the extracellular pH is high (i.e., closed-channel conformation).¹ The S31N mutant was studied mainly because it is naturally occurring and drug-resistant and there is a large amount of experimental data for comparison.^{2,12,13,17,19,20,22,54} The channel was embedded in the DPPC lipid bilayer environment (shown schematically in Figure S1B, Supporting Information), with the DPPC chemical structure and its parameters shown in Figure S2A, Supporting Information), as the pre-equilibrated DPPC structure is available^{36,37} and has been widely used in MD simulations.²³ In addition, at this pH, rimantadine should be mostly protonated in water,⁵⁵ at the lipid–water interface,⁵⁶ and inside the M2 channel pore or at the C-terminal surface binding site, on the basis of pK_a calculations (details are given in the Supporting Information, including Table S1). As a result, only protonated rimantadine (Figures S1C and S2) was considered in this study.

We then performed 21 ns MD simulations (6 ns under constraints and 15 ns unconstrained) for these six structures (Table 2). The backbone rmsd values leveled off around 3.0 Å after ~4 ns of unconstrained MD (Figure S3, Supporting Information), and the α helix bundle remained stable in the closed-channel conformation throughout the simulation. In addition, both pore binding rimantadine and surface binding rimantadine molecules were found to be stably bound at these sites during the simulation of the wild type M2 channel.

More detailed structural analyses that are presented below demonstrate the reliability and accuracy of the modeled structures of our simulation. We note that although our starting structure (solution NMR, PDB ID 2RLF) was symmetric, during the MD simulation, the M2 transmembrane α helices and the helix bundle became somewhat tilted from the membrane normal and the channel structure became asymmetric (summarized in the Supporting Information) for the six simulated structures, which agrees well with similar studies.^{23,57}

3.1.2. Pore Radii of the Model Structures. Figure 2 summarizes the average channel pore radii (and standard deviations) along the pore helix in all six structures studied here. The two ends of the transmembrane domain are found to form two constricting “gates”, and inside the N-terminal gate there is a large cavity

(see also Figure S4, Supporting Information), consistent with previous studies.^{15,26,27,31}

From Figure 2, we found that pore binding of rimantadine increased the channel pore radius around the N-terminal gate and in the vicinity of Gly34 in comparison with that of the apo form for both the wild type and the S31N mutant. In addition, we also found that rimantadine binding in the pore caused the C-terminal part of the channel to become less flexible compared to that of the apo form (smaller standard deviations of pore radii), suggesting that drug binding in the pore affects the C-terminal conformation of the M2 channel allosterically. The S-binding rimantadine molecules, on the contrary, decreased the pore radii of the M2 channel in the pore region.

Among the apo, P-binding, and S-binding forms of the simulated structures, the pore radii around Gly34 of only the P-binding form are in agreement with the solution NMR structure²⁷ (PDB ID 2RLF) (about 3 Å), whereas the pore radii of the S-binding and apo forms are ~ 1 Å smaller. This result suggests that a rimantadine molecule may be present in the channel pore of the solution NMR structure but was not detected. We will discuss this result further in the following section.

3.1.3. P-binding Model of the M2–Drug Complex. In the simulation of the P-binding M2–drug complex, rimantadine was found to lie below Val30 with its ammonium group pointing to the C-terminal portion of the channel, consistent with previous work.^{17,26,33,58} The vertical axis of rimantadine (Figure S1C, Supporting Information) tilts by $\sim 30^\circ$ from the membrane normal (Figure S5, left panel, Supporting Information). Similar tilt angles have been observed in both ssNMR experiments and molecular dynamics simulations for amantadine.¹⁵ Hydrogen bonds were previously observed between amantadine's ammonium group and the His37 residues^{3,21,59} at neutral environmental pH. In our simulations, hydrogen bonds were found between the drug molecule's ammonium group and the side chains of all four His37 residues, which indicates that the rimantadine molecule may be spinning in the channel lumen. Rotation of pore binding rimantadine was verified by monitoring its orientation during the simulation as shown in Figure S6, Supporting Information (see also Figure S5, right panel). Similar rotation has been observed for pore binding amantadine.^{32,33}

For both the wild type and the S31N mutant, comparable results were obtained for the tilt angle and the rotation of rimantadine (Figure S5, Supporting Information). However, the average number of hydrogen bonds between the rimantadine and the four His37 residues is 0.3 for the wild type and 0.1 for the S31N mutant, suggesting that the drug's binding affinity to the M2 channel may be decreased in the mutant.

Stouffer et al.¹³ and Cady et al.³³ proposed that rimantadine might be bound to the channel pore in the solution NMR structure²⁷ but was not detected due to its rapid rotation. The pore radius results (Figures 1 and 2) as well as our observation of rotation of the P-binding rimantadine (Figures S5, right panel, and S6, Supporting Information) support this hypothesis. As a result, it is highly possible that the solution NMR structure actually contained both P-binding and S-binding rimantadine molecules, suggesting that the solution NMR drug concentration was high enough to cause saturation of both binding sites.

3.1.4. S-binding Model of the M2–Drug Complex. For the S-binding M2–rimantadine complex structure, we found that the drug molecules formed extensive hydrophobic interactions with Leu40, Ile42, and Leu43 of M2 using its adamantane group

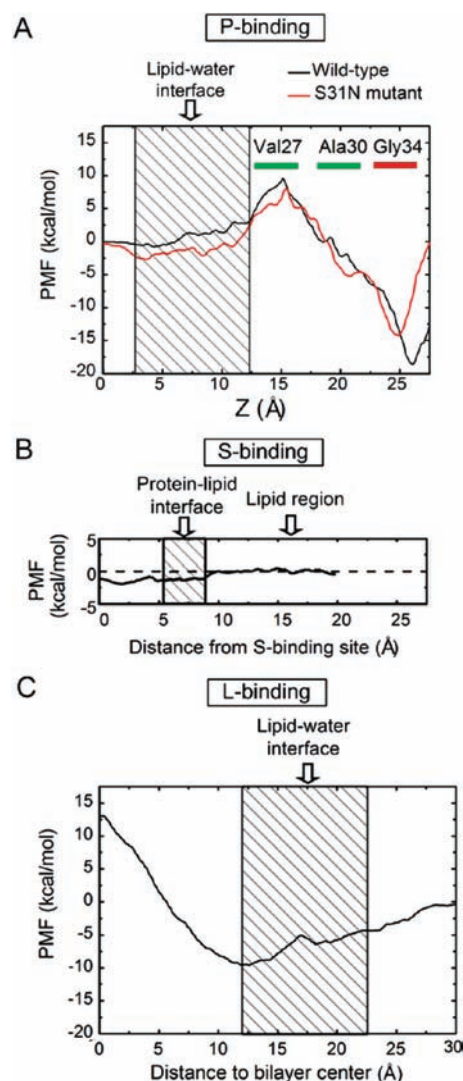


Figure 3. PMF profiles for three rimantadine binding sites in the M2–lipid environment. These results were calculated using the GRO-MOS united-atom force field (for the protein and rimantadine) and Berger's force field (for lipids). Panel A shows the pore binding PMF of a rimantadine molecule entering the channel pore from the N-terminal end, with the wild type in black and the S31N mutant in red. Panel B shows the PMF of a rimantadine molecule leaving the surface binding site and entering the lipid–water environment. Panel C shows the PMF of a rimantadine molecule entering the lipid bilayer from the solvent. The shaded regions in panels A and C represent the lipid–water interface, where both water molecules and lipid head groups are present. The protein–lipid interface and the lipid region are labeled in panel B.

(Table S2, Supporting Information), consistent with the solution NMR structure.²⁷ Rimantadine molecules also formed hydrogen bonds with polar residues (Asp44 and Arg45) of the M2 channel protein. For the wild type channel, the average numbers of hydrogen bonds between the four drug molecules and the M2 channel throughout the simulation are 0.276, 0.821, 0.109, and 0.162, respectively. For the S31N mutant, the numbers are 1.232, 0.290, 0.004, and 0.001, respectively. The drug molecules also formed hydrogen bonds simultaneously with the lipid head groups and water. The average hydrogen bond numbers are 1.5 ± 0.1 (with protein), 1.0 ± 0.1 (with lipid), and 3.0 ± 0.2 (with water) for both the wild type and the S31N mutant. In

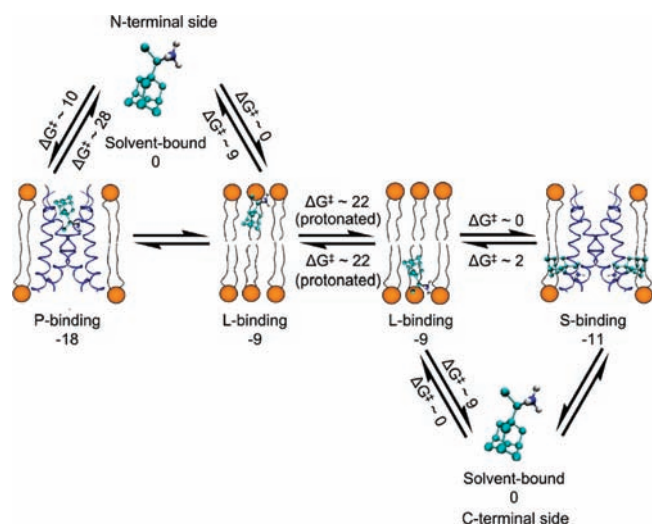


Figure 4. Free energy values for the four binding states of rimantadine in the M2–lipid environment. The solvent-bound state is used as the reference state whose binding free energy value is zero. The two drug binding sites in the M2 channel (P-binding and S-binding), the lipid binding state, and the solvent-bound state are shown. The free energy changes and the activation barriers (ΔG^\ddagger) (both in kilocalories per mole) associated with the transitions between these states estimated from the potential of mean force calculations (Figure 3) are indicated, with the binding free energy labeled below the name of each state and the energy barrier labeled above or below the arrow that represents the state transition. Rimantadine molecules are shown in the ball-and-stick representation, whereas proteins are shown in the ribbon representation.

addition, the four drug molecules have slightly different binding orientations during the simulation (Figure S7, Supporting Information).

The extensive interactions between the S-binding rimantadine molecules and the M2 channel, together with the fact that these rimantadine molecules caused a narrowing of the channel pore (Figure 2), strongly support Chou group's hypothesis that S-binding drug molecules stabilize the closed channel by affecting the rest of the protein's conformation allosterically.^{27,28}

Although similar drug orientations and binding patterns were found for the wild type and the S31N mutant for the S-binding model, it appears that the fourth rimantadine molecule has few hydrophobic interactions (Table S2, Supporting Information) or hydrogen bonds with the M2 channel in the mutant. This particular rimantadine molecule was found to primarily interact with the lipids and water nearby, as well as with the amphipathic C-terminal base of the M2 channel. In the solution NMR structure of the S31N mutant,²⁸ the mutation affected the C-terminal conformation of the protein, resulting in ineffective rimantadine binding. In comparison, our simulation suggests that, in the lipid bilayer environment, the degree of conformational change in the M2 channel and the impact on rimantadine binding by the S31N mutation are rather small and limited to one drug molecule. This difference between our results and the solution NMR structure may be due to the flexibility of the M2 channel structure, which is highly dependent on its environment.

3.2. Potential of Mean Force Calculations. Drug binding to the M2 channel protein can be considered a chemical reaction. In this reaction, the drug molecules need to be positioned and oriented in a way that facilitates the formation of favorable hydrophobic interactions and hydrogen bonds with the M2 channel. The

reaction rate of forming an M2–drug complex is dependent on the activation energy barrier of this binding reaction that the drug must overcome, according to the Arrhenius equation. Once bound to the channel, the drug molecules may dissociate, the ease of which depends on the energy barrier of the reverse dissociation reaction. Therefore, calculating potentials of mean force for drug molecules as they bind to the M2 channel will provide important energy information that may reveal which binding site (P-binding or S-binding) may lead to drug binding more easily (kinetic binding) and more stably (thermodynamic binding). On the basis of these considerations, we computed the PMFs associated with the P-binding and S-binding sites.

We note that, in the M2–bilayer environment, drug molecules may bind to the lipid–water interface, in addition to binding to the M2 channel. Chew et al.⁵⁶ and Li et al.¹⁴ found that amantadine and rimantadine can bind favorably to lipid bilayers at the lipid–water interface (L-binding model) and proposed that the lipid-bound state is prevalent and important for in vivo drug delivery and efficacy considerations. Chew et al.⁵⁶ also found that, at biological pH (~ 7.4), the amantadine and rimantadine molecules are mostly protonated in water or at the lipid–water interface, but may become easily deprotonated once inside the lipid bilayer, which would facilitate the transport of the drug molecules across membranes at very low energy cost. On the basis of their results as well as drug absorption and concentration studies in vivo,⁶⁰ it is believed that, once administered to the human body, the drugs may easily enter infected cells (such as the cells in the respiratory system as shown in ref 60) by crossing cell membranes to reach viral particles inside the cell. Therefore, drug molecules would have access to both the channel pore binding site and the C-terminal surface binding sites for M2 channel inhibition in vivo. Our study, therefore, assumes that drug molecules are populated at both sides of the lipid bilayer and the formation and stability of the M2–drug complex for either the P-binding model or the S-binding model are solely dependent on the reaction energy barrier and the depth of the free energy well, respectively.

In the P-binding PMF calculation, we studied the free energy change along the channel helix as a rimantadine molecule moves from the solvent phase at the N-terminal end to the inside of the channel pore. Figure 3A (black line) summarizes the PMF results. We found that, to enter the channel pore, a rimantadine molecule needs to overcome an energy barrier of about 10 kcal/mol at the channel N-terminal entrance (i.e., around Val27 and Ala30). Afterward, the drug may be stably bound around Gly34 (the P-binding site) in a deep energy well of about -18 kcal/mol (Figure 3A). The reverse dissociation reaction of a rimantadine molecule leaving the pore and exiting from the N-terminal end to become solvent-bound would require overcoming a high energy barrier of about 28 kcal/mol, suggesting that the P-binding M2–drug complex is very stable thermodynamically.

In the S-binding PMF calculation, we computed the free energy profile for an S-binding rimantadine molecule to dissociate and enter the lipid–water environment (the L-binding site) (Figure 3B). From Figure 3B, we found that the binding reaction of lipid-bound rimantadine and the M2 channel to form the S-binding M2–drug complex does not have an energy barrier. The energy well for the bound complex is shallow with a binding energy change of only -2 kcal/mol from the L-binding site, suggesting that the reverse dissociation reaction only has a 2 kcal/mol energy barrier to overcome. These results suggest that the S-binding site is kinetically more favorable, as close-by drug molecules at the lipid–water interface can easily bind to the

channel at this site. However, the drug molecule is not very stably bound and may dissociate fairly easily into the lipid–water environment.³²

In the lipid binding PMF calculation, we computed the PMF of a protonated rimantadine molecule as it enters the lipid bilayer from the solvent. We found that the drug molecule reached an energy well of about -9 kcal/mol at the boundary of the lipid bilayer and the solvent (the L-binding site). The energy barrier for reaching the center of the bilayer is about 22 kcal/mol (Figure 3C). These results are in excellent agreement with Chew et al.'s findings in POPC bilayers.⁵⁶

The PMF results are summarized in Figure 4. Four possible states of the drug exist in the M2–lipid bilayer system: the solvent-bound state, the L-binding state, the P-binding state, and the S-binding state. Among these four states, the solvent-bound and L-binding states exist at both the N-terminal and C-terminal sides of the M2 channel. If we assign the free energy of the solvent-bound state of rimantadine a value of zero, then the free energies of the P-binding, S-binding, and L-binding rimantadines would be -18 , -11 , and -9 kcal/mol, respectively. Similarly, if the L-binding state is used as the reference state, the binding free energies for the P-binding and S-binding rimantadines would become -9 and -2 kcal/mol, respectively. On the basis of Rosenberg et al.'s³⁰ dissociation constant (K_D) results and the formula $\Delta G_D = -RT \ln K_D$, in the liposome environment, the binding free energies of the P-binding and S-binding sites would be -9 and -4 kcal/mol for rimantadine, respectively. These results are in good agreement with our free energy calculations, if the lipid binding state is used as the reference point.

To evaluate the effect of the choice of force fields on the accuracy of our free energy calculations, we repeated the MD simulations and the PMF calculations for the wild type P-binding and S-binding models using the OPLS all-atom force field for describing the protein and the rimantadine molecules (Table S3 and Figure S8, Supporting Information). We found that the OPLS all-atom force field⁴⁸ led to PMF results slightly different from those of the GROMOS united-atom force field.³⁹ For instance, the energy barrier of entering the P-binding site from the N-terminal solvent phase is about 2 kcal/mol lower than that obtained using the GROMOS united-atom force field. In addition, lower binding energies for both the P-binding and S-binding models were obtained, which were ~ 4 kcal/mol more stable than the values obtained using the GROMOS united-atom force field for protein and rimantadine description. The lower energy barrier and the deeper energy wells suggest that the OPLS all-atom force field is probably better at describing the flexibility of the protein and the induced-fitting process of drug–M2 binding, hence the lower energy values. Nonetheless, the relative binding energies of the P-binding model and the S-binding model were found to be the same, with the P-binding site being ~ 7 kcal/mol more stable than the S-binding model by both force fields. Another consistent result between the two force fields is that the formation of the S-binding state from the lipid binding state has an energy barrier of zero, indicating the ease of the formation of the S-binding state from the lipid binding state. In short, the agreement of the PMF results between the OPLS all-atom force field and the GROMOS united-atom force field is excellent and suggests that the P-binding site may be the thermodynamically favored site and the S-binding site may be the kinetically favored site.

If the majority of rimantadine molecules remain lipid-bound,⁵⁶ the surface binding site would appear to be the more easily accessed for drug binding. However, stable drug binding and

channel inhibition likely occurs at the pore binding site due to its more favorable binding free energy, consistent with several previous studies.^{29,30,33} We propose that the differences among experimental results regarding these binding sites may be due to differences in the protein chain length used in the study, environmental pH, and, more importantly, conditions that favor either thermodynamic binding (under equilibrium conditions or low drug concentrations) or kinetic binding (nonequilibrium conditions or high drug concentrations) of the drug molecules. Additional experimental work on the full-length M2 protein, such as single-molecule experiments, which helps pinpoint the exact location of drug molecules would be helpful to determine whether *in vivo* drug binding occurs thermodynamically at the P-binding site or kinetically at the S-binding site.

For the pore binding model, the drug's bulk size and the need for dehydration of its charged ammonium group upon entering the channel pore have been considered the cause for slow drug binding and channel inhibition.^{1,59,61} Our PMF results provide energetic evidence as to why rimantadine binds and inhibits the M2 channel slowly. First, the drug molecules predominantly reside in the energy well of the lipid binding site. From the equilibrium depicted in Figure 4, the drug molecule needs to overcome two consecutive energy barriers, 9 kcal/mol for entering the solvent, and then 10 kcal/mol for entering the channel pore, before forming the P-binding M2–drug complex. These high energy barriers would lead to slow binding and inhibition.

3.3. Drug Resistance in the S31N Mutant. Figure 2 shows that the S31N mutation caused an increase of the pore radii around the N-terminal hydrophobic gate by about 0.7 Å in all three forms of the channel. This result agrees with the solution NMR structure of the S31N mutant (PDB ID 2KIH) where the pore radii around Ala30 are greater than those of the wild type (PDB ID 2RLF) (Figure 1). In our simulations, we found that the side chain of Ser31 was located at interhelical interfaces, which is consistent with the solution NMR structures and recent ssNMR³³ and IR experiments.⁶² The mutation from Ser to the larger Asn residue thus pushed the helices out and created a larger cavity. The larger pore radii in the S31N mutant may lead to easier entry and binding of rimantadine in the channel pore and much easier dissociation, thus causing insufficient channel occlusion for inhibition. This hypothesis was supported by our PMF calculation for the mutant (Figure 3A, red line, lower energy barrier and shallower energy well than those of the wild type). The less favorable M2–drug binding in the mutant is consistent with our observation of fewer hydrogen bonds between the rimantadine and the His37 residues in the S31N mutant.

However, the above drug resistance mechanism of S31N mutant is inconsistent with some experimental results. Among the 10 experimental M2 structures (Table 1), Ser31 was found to participate in helix packing in the most recent solution and solid-state NMR structures (PDB IDs 2H95, 2RLF, and 2KIH), but was found to point toward the channel lumen in the crystal structure²⁶ and some earlier NMR structures. The S31N mutation will increase the pore radii of the P-binding site if Ser31 lies at the interhelical interfaces, but will decrease the pore radii if Ser31 points to the channel lumen. Astrahan et al.⁵⁴ and Rosenberg et al.³⁰ found that the S31N mutant channel no longer binds with amantadine, consistent with Ser31 pointing toward the channel lumen. However, only the transmembrane domain of the M2 protein was included in these studies. Due to the protein

flexibility and the difference in experimental conditions and protein lengths, we believe that the drug inhibition mechanism of the S31N mutant remains a complex problem that requires further experimental and computational investigations, preferably on the full-length M2 protein.

4. CONCLUSIONS

We carried out molecular dynamics simulations and potential of mean force calculations on the M2–rimantadine complex for two alternative drug binding models: pore binding and surface binding models. From the PMF calculations for the two drug binding models, we found that pore binding requires a high energy barrier to be overcome but is thermodynamically favorable, leading to stable drug binding and inhibition. In comparison, the less energetically stable surface binding site can be easily accessed by rimantadine molecules in the lipid–water environment. These results complement existing work, expand our understanding of these binding sites, and may help guide drug design and screening studies.

There are many important open questions about the M2 channel that require continued research. For instance, our simulation was done at neutral pH. How the channel structure would change its conformation at low pH and consequently affect drug binding needs additional study, especially for the full-length protein. For another example, we have only investigated the PMF of rimantadine entering the channel pore from the N-terminal end. There is a possibility that a rimantadine molecule may first associate with an M2 monomer, which later assembles into an M2–rimantadine tetramer complex.⁴⁶ Such a binding reaction is out of the scope of the current study, but is worth additional exploration. Finally, two recent papers^{52,63} proposed two different proton conduction mechanisms of the M2 channel inferred from NMR experiments, highlighting that, despite its seeming simplicity, the M2 channel is actually a rather complex system due to its plasticity and sensitivity to its environment,^{64–69} which calls for continued and thorough investigations both experimentally and computationally.

■ ASSOCIATED CONTENT

Supporting Information. Review of the M2 channel structure and function, support of the P-binding site, support of the S-binding site, simulation protocols, potential of mean force calculations, data analysis, pK_a estimation of rimantadine in different environments, helix tilt angle and channel tilt angle calculations, sensitivity of free energy calculations to force fields, and additional figures and tables. This material is available free of charge via the Internet at <http://pubs.acs.org>.

■ AUTHOR INFORMATION

Corresponding Author

lliu2@fhcrc.org; dqwei@sju.edu.cn

■ ACKNOWLEDGMENT

We thank Jason Schnell, William DeGrado, James Chou, Philip Biggin, Amanda Stouffer, Marco Casarotto, and Hadas Leonov for insightful discussions. We thank Chris Neale for sharing parameters for combining the OPLS all-atom force field and Berger's united-atom force field. This work was supported by grants from the National Basic Research Program of China (973) under Contract

2011CB707500, the Chinese National Science Foundation under Contract No. 30870476, and the National Comprehensive Technology Platforms for Innovative Drug R&D (2009ZX9301-007).

■ REFERENCES

- (1) Wang, C.; Takeuchi, K.; Pinto, L. H.; Lamb, R. A. *J. Virol.* **1993**, *67*, 5585–5594.
- (2) Holsinger, L. J.; Nichani, D.; Pinto, L. H.; Lamb, R. A. *J. Virol.* **1994**, *68*, 1551–1563.
- (3) Pinto, L. H.; Dieckmann, G. R.; Gandhi, C. S.; Papworth, C. G.; Braman, J.; Shaughnessy, M. A.; Lear, J. D.; Lamb, R. A.; DeGrado, W. F. *Proc. Natl. Acad. Sci. U.S.A.* **1997**, *94*, 11301–11306.
- (4) Smondjrev, A. M.; Voth, G. A. *Biophys. J.* **2002**, *83*, 1987–1996.
- (5) Tang, Y.; Zaitseva, F.; Lamb, R. A.; Pinto, L. H. *J. Biol. Chem.* **2002**, *277*, 39880–39886.
- (6) Wu, Y.; Voth, G. A. *FEBS Lett.* **2003**, *552*, 23–27.
- (7) Kass, I.; Arkin, I. T. *Structure* **2005**, *13*, 1789–1798.
- (8) Pinto, L. H.; Lamb, R. A. *Photochem. Photobiol. Sci.* **2006**, *5*, 629–632.
- (9) Pinto, L. H.; Lamb, R. A. *J. Biol. Chem.* **2006**, *281*, 8997–9000.
- (10) Chen, H.; Wu, Y.; Voth, G. A. *Biophys. J.* **2007**, *93*, 3470–3479.
- (11) Luo, W.; Mani, R.; Hong, M. *J. Phys. Chem. B* **2007**, *111*, 10825–10832.
- (12) Jing, X.; Ma, C.; Ohigashi, Y.; Oliveira, F. A.; Jardetzky, T. S.; Pinto, L. H.; Lamb, R. A. *Proc. Natl. Acad. Sci. U.S.A.* **2008**, *105*, 10967–10972.
- (13) Stouffer, A. L.; Ma, C.; Cristian, L.; Ohigashi, Y.; Lamb, R. A.; Lear, J. D.; Pinto, L. H.; DeGrado, W. F. *Structure* **2008**, *16*, 1067–1076.
- (14) Li, C.; Yi, M.; Hu, J.; Zhou, H. X.; Cross, T. A. *Biophys. J.* **2008**, *94*, 1295–1302.
- (15) Yi, M.; Cross, T. A.; Zhou, H. X. *J. Phys. Chem. B* **2008**, *112*, 7977–7979.
- (16) Balannik, V.; Wang, J.; Ohigashi, Y.; Jing, X.; Magavern, E.; Lamb, R. A.; DeGrado, W. F.; Pinto, L. H. *Biochemistry* **2009**, *48*, 11872–11882.
- (17) Cady, S. D.; Mishanina, T. V.; Hong, M. *J. Mol. Biol.* **2009**, *385*, 1127–1141.
- (18) Hong, M.; Mishanina, T. V.; Cady, S. D. *J. Am. Chem. Soc.* **2009**, *131*, 7806–7816.
- (19) Ohigashi, Y.; Ma, C.; Jing, X.; Balannick, V.; Pinto, L. H.; Lamb, R. A. *Proc. Natl. Acad. Sci. U.S.A.* **2009**, *106*, 18775–18779.
- (20) Balannik, V.; Carnevale, V.; Fiorin, G.; Levine, B. G.; Lamb, R. A.; Klein, M. L.; DeGrado, W. F.; Pinto, L. H. *Biochemistry* **2010**, *49*, 696–708.
- (21) Intharathep, P.; Laohpongspaisan, C.; Rungrotmongkol, T.; Loisuangsinsin, A.; Malaisree, M.; Decha, P.; Aruksakunwong, O.; Chuenpennit, K.; Kaiyawet, N.; Sompornpisut, P.; Pianwanit, S.; Hannongbua, S. *J. Mol. Graphics Modell.* **2008**, *27*, 342–348.
- (22) Laohpongspaisan, C.; Rungrotmongkol, T.; Intharathep, P.; Malaisree, M.; Decha, P.; Aruksakunwong, O.; Sompornpisut, P.; Hannongbua, S. *J. Chem. Inf. Model.* **2009**, *49*, 847–852.
- (23) Carpenter, T.; Bond, P. J.; Khalid, S.; Sansom, M. S. P. *Biophys. J.* **2008**, *95*, 3790–3801.
- (24) Aldrich, P. E.; Hermann, E. C.; Meier, W. E.; Paulshock, M.; Prichard, W. W.; Synder, J. A.; Watts, J. C. *J. Med. Chem.* **1971**, *14*, 535–543.
- (25) Ziegler, T.; Hemphill, M. L.; Ziegler, M. L.; Perez-Oronoz, G.; Klimov, A. I.; Hampson, A. W.; Regnery, H. L.; Cox, N. J. *J. Infect. Dis.* **1999**, *180*, 935–939.
- (26) Stouffer, A. L.; Acharya, R.; Salom, D.; Levine, A. S.; Di Costanzo, L.; Soto, C. S.; Tereshko, V.; Nanda, V.; Stayrook, S.; DeGrado, W. F. *Nature* **2008**, *451*, 596–599.
- (27) Schnell, J. R.; Chou, J. J. *Nature* **2008**, *451*, 591–595.
- (28) Pielak, R. M.; Schnell, J. R.; Chou, J. J. *Proc. Natl. Acad. Sci. U.S.A.* **2009**, *106*, 7379–7384.
- (29) Chuang, G. Y.; Kozakov, D.; Brenke, R.; Beglov, D.; Guarnieri, F.; Vajda, S. *Biophys. J.* **2009**, *97*, 2846–2853.

- (30) Rosenberg, M. R.; Casarotto, M. G. *Proc. Natl. Acad. Sci. U.S.A.* **2010**, *107*, 13866–13871.
- (31) Khurana, E.; Peraro, M. D.; DeVane, R.; Vemparala, S.; DeGrado, W. F.; Klein, M. L. *Proc. Natl. Acad. Sci. U.S.A.* **2009**, *106*, 1069–1074.
- (32) Khurana, E.; DeVane, R. H.; Peraro, M. D.; Klein, M. L. *Biochim. Biophys. Acta* **2011**, *1808*, 530–537.
- (33) Cady, S. D.; Schmidt-Rohr, K.; Wang, J.; Soto, C. S.; DeGrado, W. F.; Hong, M. *Nature* **2010**, *463*, 689–692.
- (34) Kozakov, D.; Chuang, G. Y.; Beglov, D.; Vajda, S. *Trends Biochem. Sci.* **2010**, *35*, 471–475.
- (35) Morris, G. M.; Goodsell, D. S.; Halliday, R. S.; Huey, R.; Hart, W. E.; Belew, R. K.; Olson, A. J. *J. Comput. Chem.* **1998**, *19*, 1639–1662.
- (36) Patra, M.; Karttunen, M.; Hyvonen, M. T.; Falck, E.; Vattulainen, I. *J. Phys. Chem. B* **2004**, *108*, 4485–4494.
- (37) Patra, M.; Karttunen, M.; Hyvonen, M. T.; Falck, E.; Lindqvist, P.; Vattulainen, I. *Biophys. J.* **2003**, *84*, 3636–3645.
- (38) Berendsen, H. J. C.; van der Spoel, D.; Van Drunen, R. *Comput. Phys. Commun.* **1995**, *91*, 43–56.
- (39) Lindahl, E.; Hess, B.; van der Spoel, D. *J. Mol. Model.* **2001**, *7*, 306–317.
- (40) Berger, O.; Edholm, O.; Jahnig, F. *Biophys. J.* **1997**, *72*, 2002–2013.
- (41) Hess, B.; Bekker, H.; Berendsen, H. J. C.; Fraaije, J. G. E. M. *J. Comput. Chem.* **1997**, *18*, 1463–1472.
- (42) Torrie, G. M.; Valleau, J. P. *J. Comput. Phys.* **1977**, *23*, 187–199.
- (43) Beutler, T. C.; van Gunsteren, W. F. *J. Chem. Phys.* **1994**, *100*, 1492–1497.
- (44) Kumar, S.; Rosenberg, J. M.; Bouzida, D.; Swendsen, R. H.; Kollman, P. A. *J. Comput. Chem.* **1992**, *13*, 1011–1021.
- (45) Duong-Ly, K. C.; Nanda, V.; DeGrado, W. F.; Howard, K. P. *Protein Sci.* **2005**, *14*, 856–861.
- (46) Kochendoerfer, G. G.; Salom, D.; Lear, J. D.; Wilk-Orescan, R.; Kent, S. B. H.; DeGrado, W. F. *Biochemistry* **1999**, *38*, 11905–11913.
- (47) Nguyen, P. A.; Soto, C. S.; Polishchuk, A.; Caputo, G. A.; Tatko, C. D.; Ma, C.; Ohigashi, Y.; Pinto, L. H.; DeGrado, W. F.; Howard, K. P. *Biochemistry* **2008**, *47*, 9934–9936.
- (48) Jorgensen, W. L.; Tirado-Rives, J. *J. Am. Chem. Soc.* **1988**, *110*, 1657–1666.
- (49) Chakrabarti, N.; Neale, C.; Payandeh, J.; Pai, E. F.; Pomès, R. *Biophys. J.* **2010**, *98*, 784–792.
- (50) Cuesta-Seijo, J. A.; Neale, C.; Khan, M. A.; Moktar, J.; Tran, C. D.; Bishop, R. E.; Pomès, R.; Privé, G. G. *Structure* **2010**, *18*, 1210–1219.
- (51) Pielak, R. M.; Chou, J. J. *Biochem. Biophys. Res. Commun.* **2010**, *401*, 58–63.
- (52) Sharma, M.; Yi, M.; Dong, H.; Qin, H.; Peterson, E.; Busath, D. D.; Zhou, H. X.; Cross, T. A. *Science* **2010**, *330*, 509–511.
- (53) Smart, O. S.; Neduvellil, J. G.; Wang, X.; Wallace, B. A.; Sansom, M. S. P. *J. Mol. Graphics* **1996**, *14*, 354–360.
- (54) Astrahan, P.; Kass, I.; Cooper, M. A.; Arkin, I. T. *Proteins: Struct., Funct., Bioinf.* **2004**, *55*, 251–257.
- (55) Spector, R. J. *Pharmacol. Exp. Ther.* **1988**, *244*, 516–519.
- (56) Chew, C. F.; Guy, A.; Biggin, P. C. *Biophys. J.* **2008**, *95*, 5627–5636.
- (57) Schweighofer, K. J.; Pohorille, A. *Biophys. J.* **2000**, *78*, 150–163.
- (58) Hu, J.; Asbury, T.; Achuthan, S.; Li, C.; Bertram, R.; Quine, J. R.; Fu, R.; Cross, T. A. *Biophys. J.* **2007**, *92*, 4335–4343.
- (59) Gandhi, C. S.; Shuck, K.; Lear, J. D.; Dieckmann, G. R.; DeGrado, W. F.; Lamb, R. A.; Pinto, L. H. *J. Biol. Chem.* **1999**, *274*, 5474–5482.
- (60) Hayden, F. G.; Minocha, A.; Spyker, D. A.; Hoffman, H. E. *Antimicrob. Agents Chemother.* **1985**, *28*, 216–221.
- (61) Mould, J. A.; Li, H. C.; Dudlak, C. S.; Lear, J. D.; Pekosz, A.; Lamb, R. A.; Pinto, L. H. *J. Biol. Chem.* **2000**, *275*, 8592–8599.
- (62) Manor, J.; Mukherjee, P.; Lin, Y. S.; Leonov, H.; Skinner, J. L.; Zanni, M. T.; Arkin, I. T. *Structure* **2009**, *17*, 247–254.
- (63) Hu, F.; Luo, W.; Hong, M. *Science* **2010**, *330*, 505–508.
- (64) Lear, J. D. *FEBS Lett.* **2003**, *552*, 17–22.
- (65) Sakaguchi, T.; Tu, Q.; Pinto, L. H.; Lamb, R. A. *Proc. Natl. Acad. Sci. U.S.A.* **1997**, *94*, 5000–5005.
- (66) Brewer, M. L.; Schmitt, U. W.; Voth, G. A. *Biophys. J.* **2001**, *80*, 1691–1702.
- (67) Vijayvergiya, V.; Wilson, R.; Chorak, A.; Gao, P. F.; Cross, T. A.; Busath, D. D. *Biophys. J.* **2004**, *87*, 1697–1704.
- (68) Sansom, M. S. P.; Kerr, I. D.; Smith, G. R.; Son, H. S. *Virology* **1997**, *233*, 163–173.
- (69) Nishimura, K.; Kim, S.; Zhang, L.; Cross, T. A. *Biochemistry* **2002**, *41*, 13170–13177.

NOTE ADDED AFTER ASAP PUBLICATION

A production error in Table 1 has been corrected and this paper reposted on July 13, 2011.